Solid Freeform Fabrication 2017: Proceedings of the 28th Annual International Solid Freeform Fabrication Symposium – An Additive Manufacturing Conference
Reviewed Paper

Effect of Heat Treatment on the Microstructures of CMSX-4® Processed through Scanning Laser Epitaxy (SLE)

Amrita Basak[1], and Suman Das[1, 2]

[1]George W. Woodruff School of Mechanical Engineering, 813 Ferst Dr NW, Georgia Institute of Technology, Atlanta, GA 30332
[2]School of Materials Science and Engineering, Georgia Institute of Technology, 771 Ferst Dr NW, Atlanta, GA 30313

Engineered components made of superalloys routinely undergo heat treatment procedures to tailor their microstructures and properties. In this study, the effect of heat treatment on the microstructures and microhardness of single-crystal nickel-base superalloy CMSX-4® is investigated. Samples of CMSX-4® are fabricated using scanning laser epitaxy (SLE), a laser powder bed fusion (LPBF)-based additive manufacturing process. Microstructural characterizations of the as-deposited and the heat treated CMSX-4® samples are performed using optical microscopy, scanning electron microscopy, x-ray diffraction, and Vickers microhardness measurements. The results show that the microstructure is homogenized with reductions in the eutectic volume fraction after heat treatment. The microhardness values are also improved upon heat treatment. This work is sponsored by the Office of Naval Research through grant N00014-14-1-0658.

Keywords: Additive Manufacturing, Scanning Laser Epitaxy (SLE), Nickel-base, Superalloys, CMSX-4®, Heat-treatment

Introduction

The performance of gas turbines improves with increase in the operating temperature creating a hostile environment for the hot-section components. Currently, nickel-base superalloys are used to fabricate hot-section components as they offer higher yield strength with increase in operating temperatures primarily due to the presence of the secondary γ' precipitate phases that form an antiphase boundary and lock the associated dislocation movements. However, due to the rotational movements of hot-section components under very high temperature, they suffer from material losses due to thermal abrasion, corrosion, and oxidation. With several hundred such components installed in each gas turbine engine, their total replacement cost at the time of overhaul is upwards of hundreds of thousands or even millions of dollars per engine. Hence, there is a great commercial interest in developing additive manufacturing (AM)-based repair processes that are capable of restoring the parent metallurgical microstructure and geometry at damage locations.

Scanning laser epitaxy (SLE) is a laser powder bed fusion (LPBF)-based AM process that creates equiaxed (EQ), directionally solidified (DS) and single-crystal (SX) structures of nickel superalloys onto like-chemistry substrates. In SLE, a galvanometer controlled laser beam is focused upon the powder bed that generates a melt-pool. The melt-pool travels along the length of the substrate fusing the completely melted powder to the partially melted substrate. Under the proper operating conditions, the solidified microstructure has been demonstrated to follow the morphology of the underlying substrate [1]. The SLE process has shown significant potential for

one-step repair of CMSX-4® [2-4], René N5 [5, 6], René 142 [7], MAR-M247 [8], René 80 [9], and IN100 [10, 11].

CMSX-4® is a second generation ultrahigh-strength SX superalloy developed using a multidimensional approach over a ten year period through the joint efforts of Canon-Muskegon and Allison at the beginning of the 1990s [12]. The alloy demonstrates a significant improvement of 35 ºC in the turbine airfoil temperature capability compared to the first-generation SX superalloys such as CMSX-2® and CMSX-3® [13]. CMSX-4® is derived from CMSX-2® and enjoys the strengthening effects of rhenium (Re) (3 wt. %) like other second generation SX superalloys. Re partially segregates to the γ matrix, and thereby, delays coarsening of the γ′ phase [14]. CMSX-4® is strengthened by the solid-solution-strengthening effects of chromium (Cr), tungsten (W), and tantalum (Ta) and the precipitation-hardening effects of aluminum (Al) and titanium (Ti) that form the γ′ phase [12].

Although CMSX-4® has excellent thermo-mechanical properties, heat treatment via aging (below 1090 ºC) or solutioning (above 1090 ºC) and aging is usually applied to further improve the mechanical properties. Heat treatment is instrumental in reducing elemental segregation. Heat treatment procedures also refine the dispersion of γ′ phases and decrease the amount of γ/γ′ eutectics. Additionally, carbide precipitates are also redistributed during heat treatment and re-precipitate at the grain boundaries [8]. In the present work, SLE deposited CMSX-4® samples were subjected to heat treatment via aging. In order to relieve the residual stresses and enable precipitation of the strengthening phases, the samples were heated and kept at 1080 ºC for an hour. Thereafter, the samples were cooled at 5.6 ºC /minute or faster to a temperature below 900 ºC. Samples were then given a typical commercial low-temperature precipitation heat-treat cycle consisting of 4 hours at 900 ºC, followed by air cooling at minimum average cooling rate of 5.6 ºC / minute to 650 ºC to fully develop the strengthening phases. The microstructures of the as-deposited and the heat-treated samples were analyzed using optical microscopy (OM) and scanning electron microscopy (SEM), and the results are reported.

Materials and Methods

Powder of nickel-base superalloy CMSX-4® produced by the Praxair Surface Technologies through argon gas atomization was used in this study. The composition of the powder is reported in Table I. The powder was deposited on investment-cast CMSX-4® substrates. The morphology and the cross-section of powder were analyzed using OM and SEM. The CMSX-4® powders were mostly spherical, although some irregularity in shape was found as shown in Fig. 1(a). The powder was mounted in Bakelite and polished to a mirror finish. The cross-section was analyzed under an optical microscope for the inspection of internal porosity, and no major internal porosity was detected as shown in Fig. 1(b).

Table I. Chemical composition of the CMSX-4® powder (wt. %)

	Cr	Co	Mo	Re	W	Al	Ti	Ta	Ni
CMSX-4®	6.5	9.7	0.4	3.0	6.4	5.6	1.0	6.5	Bal

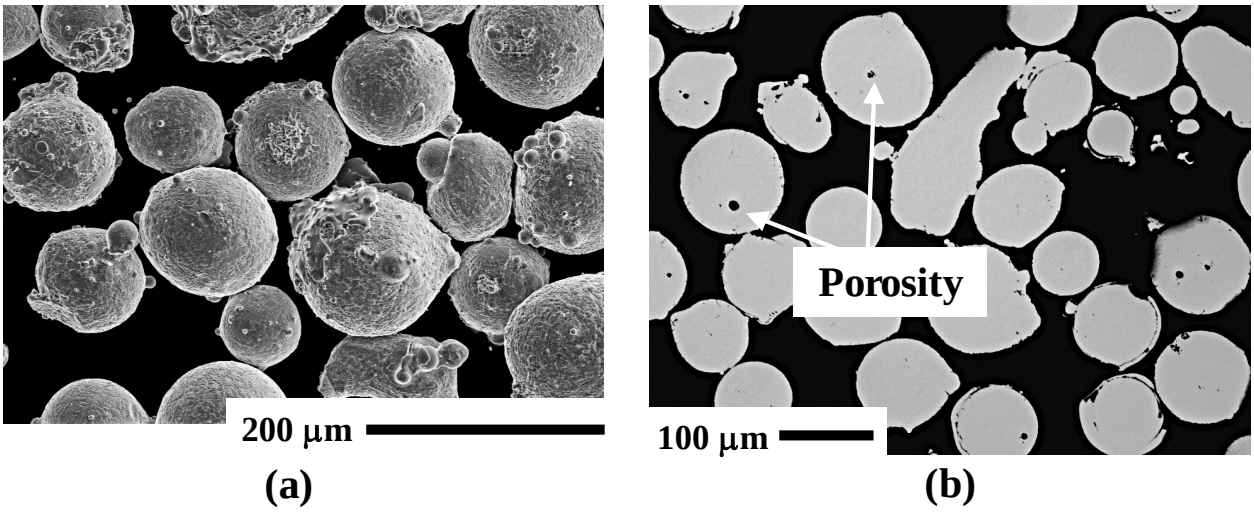

Fig. 1. (a) SEM image of the CMSX-4® powder and (b) OM image of the CMSX-4® powder cross-section after polishing.

SLE processed samples were sectioned along the length and width for the inspection of the microstructure. A Buehler automated saw was used to section the samples. The first half was retained while the second half was subjected to heat treatment. Each section was mounted in Bakelite and polished to a mirror finish; starting with 80 grit paper and progressively increasing the size to 1200 grit. The samples were then rough-polished using 5 μm and 3 μm diamond solutions. Finally, the samples were fine polished using a 0.5 μm colloidal alumina suspension. The polished samples were then etched with Marble's reagent (50 ml HCl, 50 ml H_2O, and 10.0 gm $CuSO_4$) to eliminate the γ′ phase and reveal the dendritic microstructure. A Leica DM6000 optical microscope was thereafter used to take the images. The microstructural investigation of the SLE processed CMSX-4® was carried out on a Hitachi SU8230 SEM. The SEM was equipped with an Oxford Instruments' Aztec Energy EDX system which was used for elemental analysis. Vickers microhardness measurements were carried out using a Buehler microhardness indenter with a fixed load at 2000 gf. The hardness values were extracted in Vickers microhardness scale (HV). Details on hardness measurements may be found elsewhere [11].

SLE Experimental Procedure

The SLE process was conducted on rectangular investment-cast SX CMSX-4® substrates having dimensions of 38.10 mm x 11.85 mm x 2.54 mm. Each substrate was placed into a 38.10 mm x 11.85 mm recess cut into an IN625 base plate. The CMSX-4® powder was placed above the substrates using rectangular wells cut into an Aluminum mask plate. Once the samples were prepared, they were placed into an atmospheric process chamber that was purged with high purity (99.999%) Argon. A 1kW Ytterbium fiber laser (IPG Photonics, Model: YLS-1000) was used with a Cambridge Technologies galvanometer scanner to focus the beam on top of the substrate to a Gaussian beam diameter of 40 μm. A raster scan pattern across the width of the sample generated a melt pool that linearly propagated along the length of the substrate. All the samples were run with 25.4 μm scan spacing.

Results and Discussion

Fig. 2 shows the length-wise cross-sectional microstructure of the CMSX-4® as-deposited sample. The average deposit thickness was found to be more than 1500 μm in a single-pass. As shown in Fig. 2, very few pores were observed. The deposit was also crack-free and dense. The deposit region showed a finer microstructure compared to the substrate region as shown in Fig. 2. The microstructural refinement might be attributed to the localized heating and fast cooling due to the high-speed laser heat source.

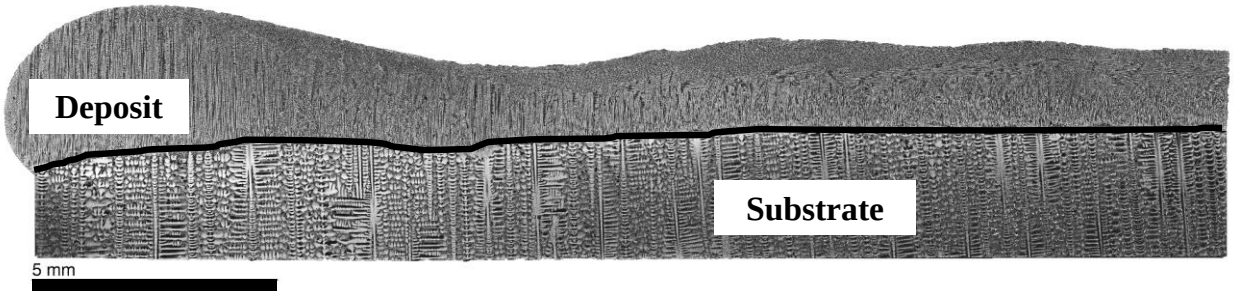

Fig. 2. Representative transverse OM image of the as-deposited CMSX-4® sample showing crack-free and dense deposit. The black line represents the substrate-deposit interface.

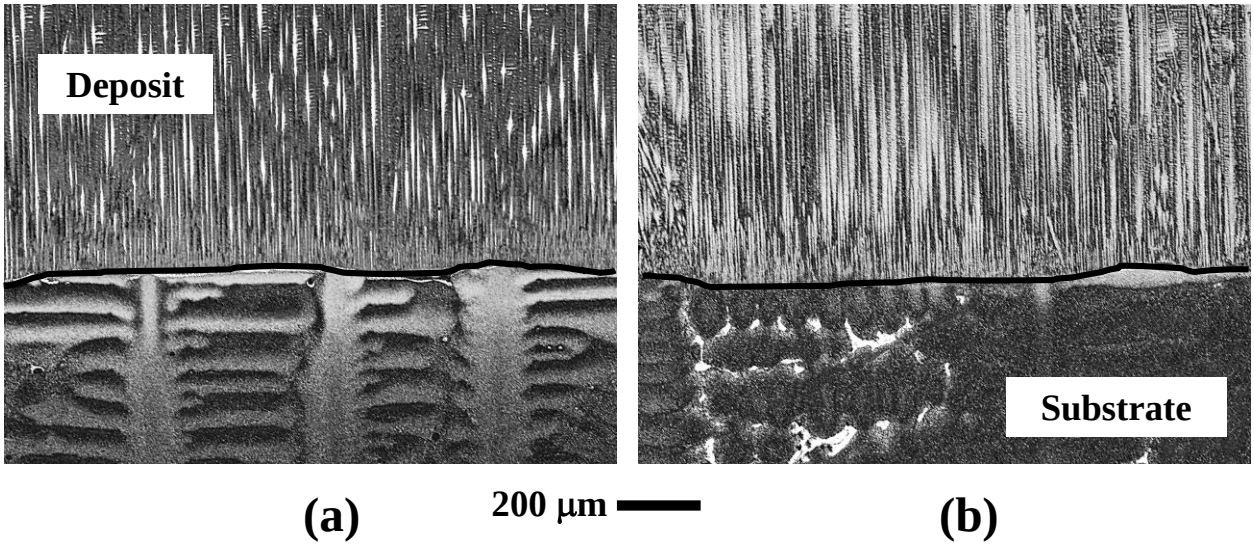

Fig. 3. OM image showing interface microstructure (a) of the as-deposited sample, and (b) the heat-treated sample. The black line represents the substrate-deposit interface.

The zoomed view of the substrate-deposit interface region is shown in Figs. 3(a) and 3(b) for the as-deposited and the heat-treated samples. No significant difference in the interface was observed near the interface region as shown in Figs. 3(a) and 3(b). The microstructure of as-deposited CMSX-4® revealed three types of dendritic microstructures such as the [001] columnar dendrites, [100] columnar dendrites, and the equiaxed dendrites. The [001] columnar dendritic microstructure grew epitaxially from the partially re-melted grains of the substrate as shown in

Fig. 3(a). The microstructure of the deposited CMSX-4® retained the columnar structure after the heat treatment as shown in Fig. 3(b).

The major constituents of the SLE processed microstructure of CMSX-4® were the γ matrix, the γ′ precipitates in the γ matrix, and the eutectics. Figure 4(a) illustrates an SEM image of the deposit region showing the major constituents in an as-deposited sample. Figure 4(b) illustrates the major constituents in the SLE deposited CMSX-4® after heat treatment. The eutectic volume fraction is visibly reduced after the heat treatment process as shown in Figure 4(b). However, after the heat treatment additional phases were found to be formed in the deposit region as shown in Fig. 4(b).

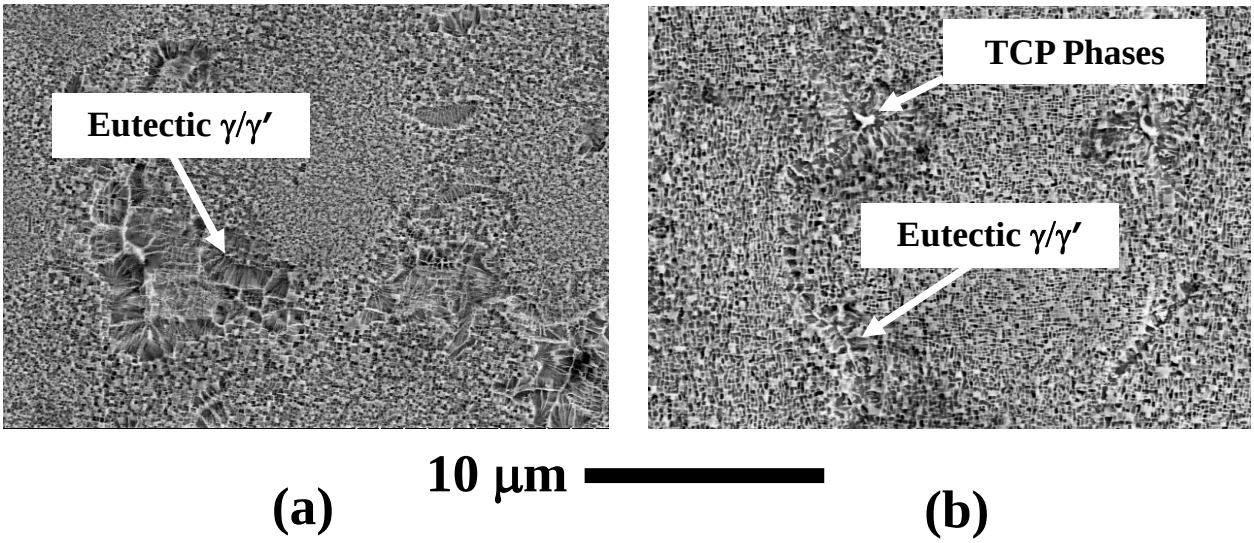

Fig. 4. SEM image showing morphologies of various constituents of SLE processed CMSX-4® deposit – (a) as-deposited sample and (b) heat-treated sample.

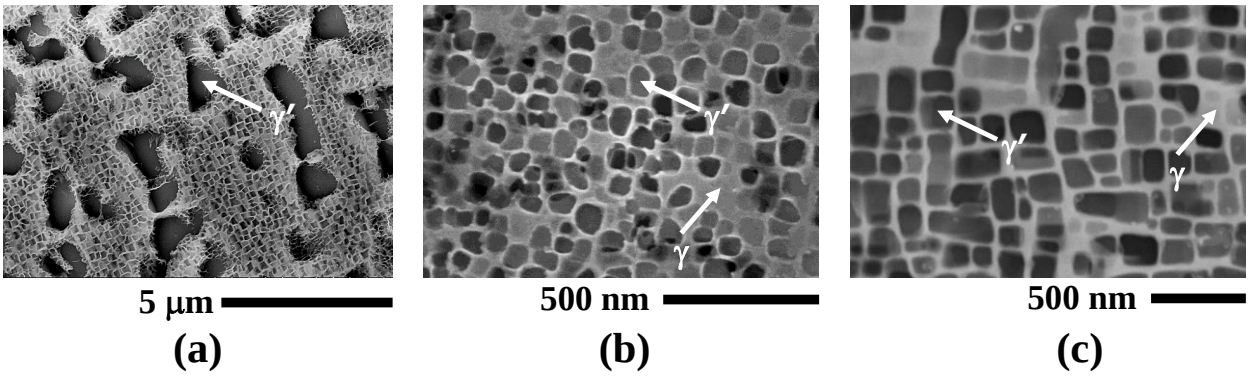

Fig. 5. Representative SEM image showing γ/γ′ morphology in the (a) substrate region, (b) deposit region of the as-deposited sample, and (c) deposit region of the heat-treated sample.

As shown in Fig. 5(a), the primary γ′ precipitates showed a characteristic dimension in the range of 2 μm in the substrate region whereas in the deposit region, the γ′ precipitates in the range of 50 nm as shown in Fig. 5(b). The deposit region shows approximately 25% reduction in the

γ′ size for the as-deposited sample. Microstructural refinement in the deposit region is visible from Figs. 5(a) and 5(b). Fig. 5(c) illustrates the γ′ size distribution in the heat-treated sample. The primary γ′ size is of order 100 nm in the heat-treated samples. The heat-treated CMSX-4® showed predominantly cuboidal precipitates as compared to polygonal shaped precipitates in the as-deposited sample as shown in Figs. 5(b) and 5(c).

To compare the size of the primary γ′ precipitates, their equivalent diameters were calculated. The equivalent diameter is defined as $D= (A/\pi)^{0.5}$, where A is the area of a γ′ precipitate determined by measuring the perpendicular sides of an individual precipitate. The average equivalent diameter, <D>, is calculated by the mean of ~100 γ′ precipitates. Fig. 6 illustrates the γ′ particle size distribution (PSD) with the theoretical Lifshitz-Slyozov-Wagner (LSW) [8] distribution superimposed for the as-deposited and heat-treated CMSX-4® samples. The normalized diameter ϕ is defined as D/<D>. The SLE processed PSD of the γ' precipitate differs considerably from the theoretical LSW distribution. This might be due to the fact that the size of the γ′ precipitates in the interdendritic regions was found to be larger than those present within the dendrite region. Note that while performing this calculation, the γ/γ′ precipitates in the eutectic pools were not considered. The γ′ size showed a closer match to the theoretical PSD for the heat-treated sample.

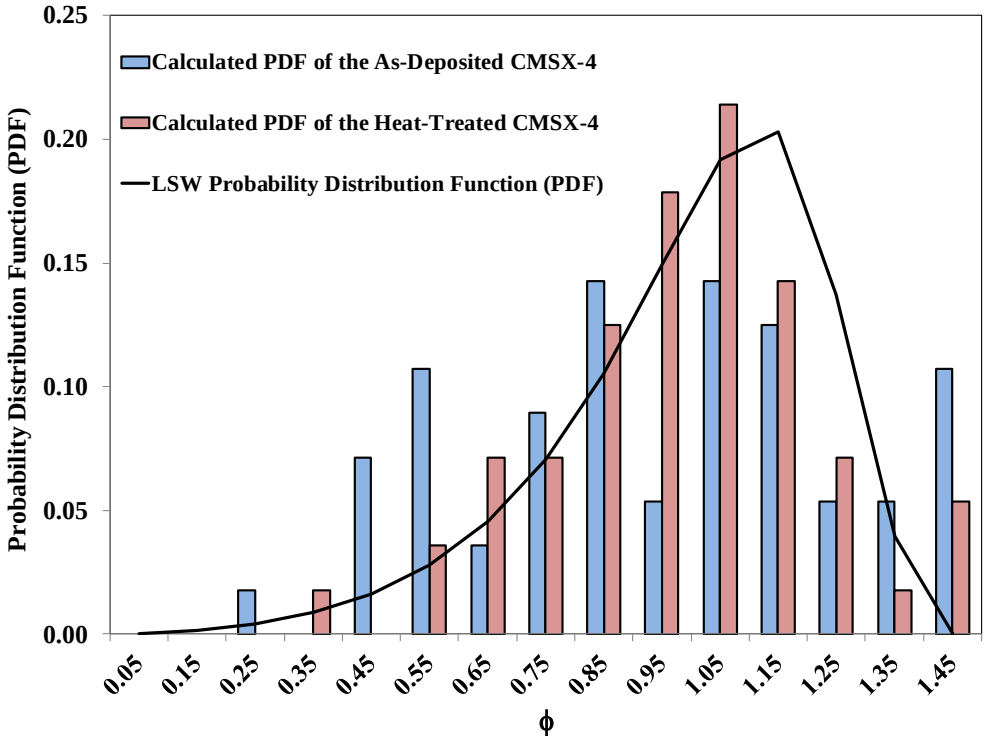

Fig. 6. Particle size distribution (PSD) of the γ′ precipitates – as-deposited and heat-treated sample.

Fig. 7(a) shows SEM images of secondary phase precipitates that were formed after the heat treatment. These precipitates were identified as topologically-closed-pack (TCP) phases. The size of these precipitates were of order 500 nm. These precipitates were observed to line up along the grain boundary surrounded by the γ′ phase. The elemental EDS maps of these particles are shown in Figs. 7(b) through 7(d). The precipitates were found to be rich in W, Re, and Cr.

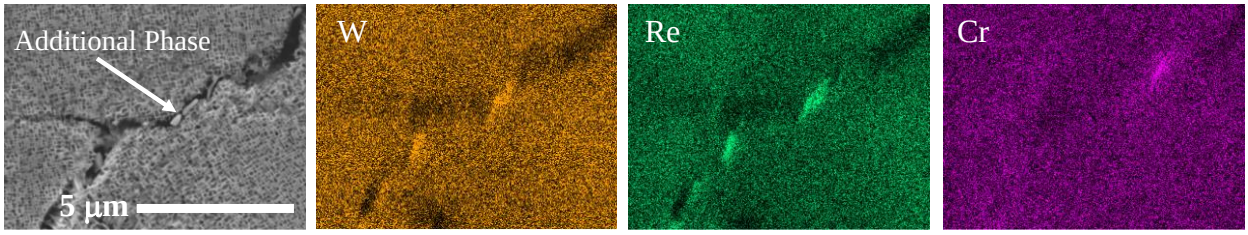

Fig. 7. (a) Representative SEM image showing morphology of the secondary phase precipitate in the CMSX-4® deposit after the heat treatment. (b)- (d) EDS Map of the precipitate.

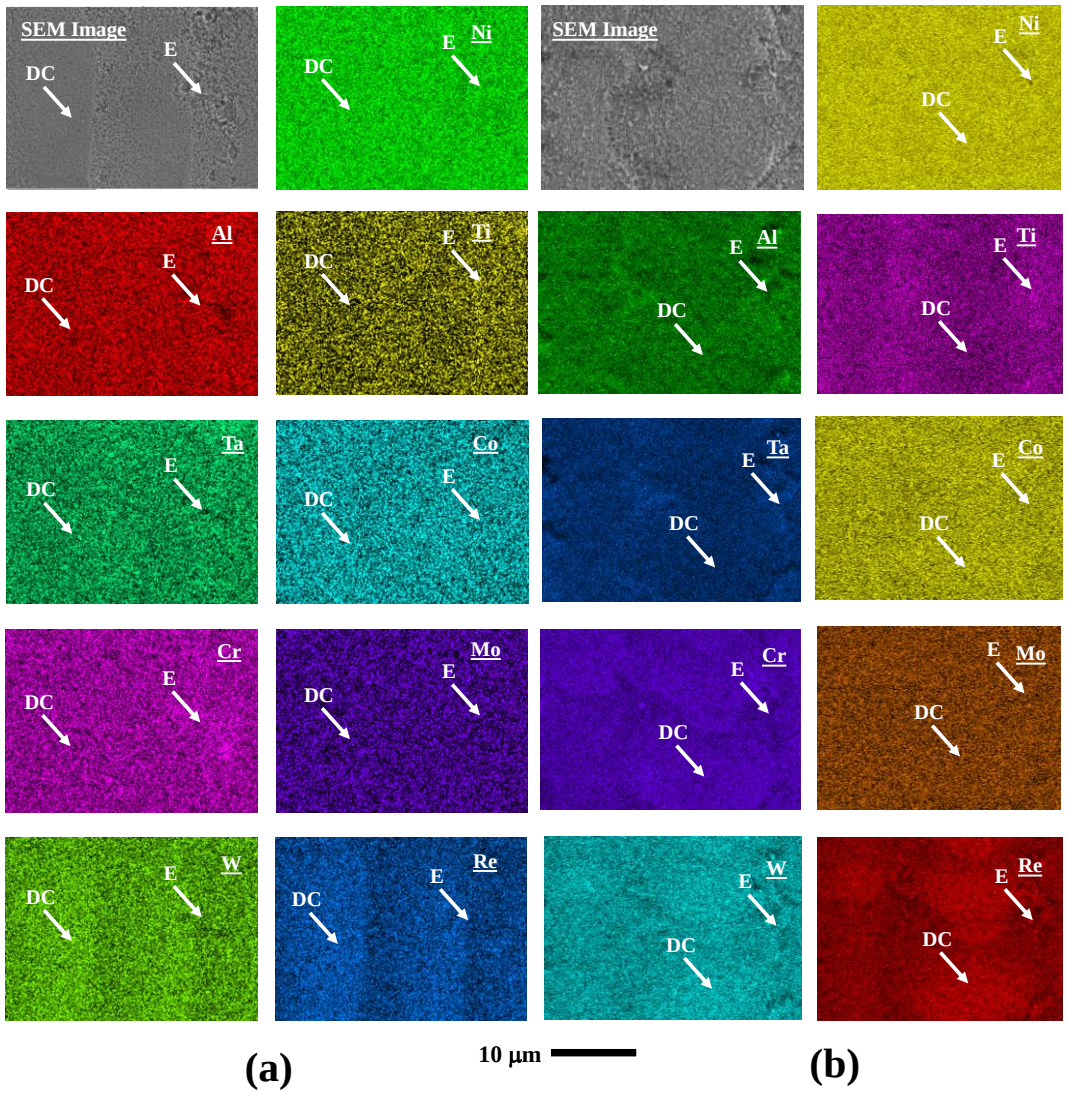

Fig. 8. SEM-EDS map of a representative region in the CMSX-4® deposit – (a) as-deposited sample and (b) heat-treated sample.

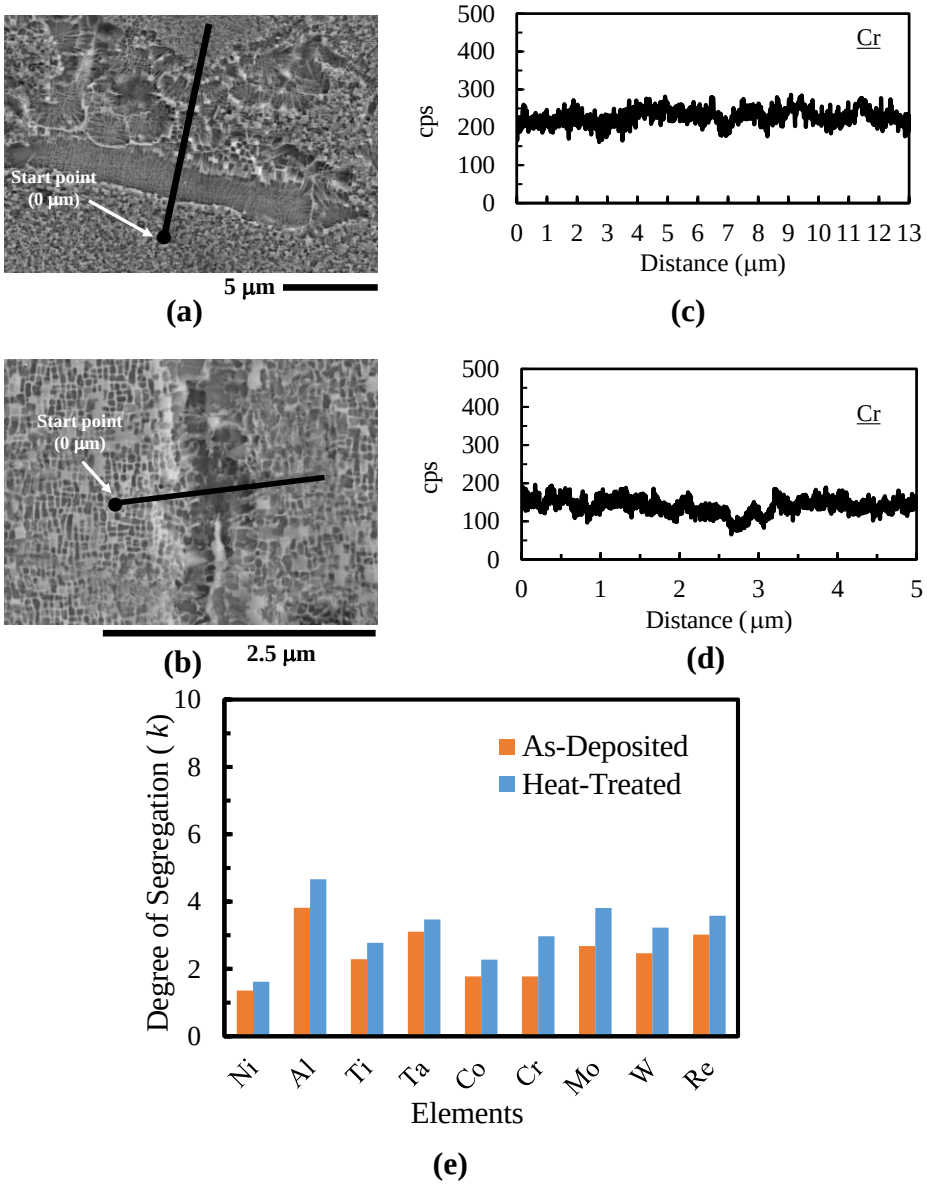

Fig. 9. SEM image of a representative line scan domain in the eutectic region of CMSX-4® deposit - (a) as-deposited and (b) heat-treated. EDS line profile of Cr across a representative eutectic region in the (c) as-deposited and (d) heat-treated CMSX-4® deposit. (f) Degree of segregation (k) of various alloying elements across representative eutectic pools in the as-deposited and heat-treated CMSX-4® sample.

Figs. 8(a) and 8(b) illustrate EDS maps of a representative region in the CMSX-4® deposit before and after the heat treatment, respectively. Note that the dendritic core and the eutectic regions are marked by DC and E, respectively. Ti and Ta showed segregation to the eutectics. W, Al, and Re showed segregation to the core (Figs. 8(a) and 8(b)). Other elements did not show any strong segregation behavior as shown in Figs. 8(a) and 8(b).

In order to quantify the elemental segregation, EDS line scans were performed across representative eutectic regions in the deposit region before and after the heat treatment,

respectively (Figs. 9(a) and 9(b)). The line profiles of a representative element (Cr) across a eutectic region in the deposit before and after the heat treatment are shown in Figs. 9(c) and 9(d), respectively. From the elemental line profiles, the maximum and the minimum counts were extracted and a segregation parameter was defined as *degree of segregation* (k) = *maximum cps/minimum cps* (where cps denotes counts per second). The k values for various elements are plotted in Fig. 9(e) for the deposit region before and after the heat treatment. Although, in comparison to the as-deposited sample, the γ/γ' eutectic phase showed increased elemental segregation for the heat-treated CMSX-4®, the dimension of the eutectic pools was significantly smaller in the heat-treated sample.

The hardness of an alloy is a strong function of the γ' size, distribution, and volume fraction and the residual stresses generated during the laser processing. In the present study, microhardness results indicated a hardness value in the range of 430-500 HV in the deposit region. The heat-treated CMSX-4® showed 10% increase in the hardness values as reported in Table II. This increase may be attributed to the uniform γ' distribution obtained after the heat treatment. The yield stress was approximated as, $\sigma_y \sim HV/3$ (HV measured in GPa) [8]. Table II shows the calculated yield stress for the as-deposited and the heat-treated CMSX-4® samples [8].

Table II. Summary of microhardness results for CMSX-4®.

Sample Type	Region	HV_{2000}	HV (GPa)	σ_y (GPa)
As-Deposited CMSX-4®	Substrate	400	3.92	1.30
	Interface	423	4.15	1.38
	Deposit	464	4.55	1.51
Heat-Treated CMSX-4®	Substrate	405	3.97	1.32
	Interface	446	4.37	1.46
	Deposit	492	4.83	1.61

Conclusions

In the present study, SLE process was demonstrated to deposit dense crack-free deposits of CMSX-4® exceeding 1500 μm in a single-pass. Commercial heat treatment suited for CMSX-4® was performed. A detailed study was conducted to characterize the microstructural changes due to the heat treatment. The microstructures of CMSX-4® became uniform after the heat treatment with more than 80% reductions in the eutectic volume fraction. The heat treatment also improved the microhardness values in the deposit region. Future investigations will be carried out to characterize TCP phase formations in CMSX-4®. The effect of heat treatment on the texture and grain size distribution will also be analyzed.

Acknowledgments and Disclosures

This work is sponsored by the Office of Naval Research through grant N00014-14-1-0658. Dr. Suman Das is a cofounder of DDM Systems, a start-up company commercializing SLE technology. Dr. Das and Georgia Tech are entitled to royalties derived from DDM Systems' sale of products

related to the research described in this paper. This study could affect their personal financial status. The terms of this arrangement have been reviewed and approved by Georgia Tech in accordance with its conflict of interest policies.

References

[1] Basak A, Das S. Epitaxy and Microstructure Evolution in Metal Additive Manufacturing. Annual Review of Materials Research 2016;46:125-49.

[2] Acharya R, Bansal R, Gambone JJ, Das S. A Coupled Thermal, Fluid Flow, and Solidification Model for the Processing of Single-Crystal Alloy CMSX-4 Through Scanning Laser Epitaxy for Turbine Engine Hot-Section Component Repair (Part I). Metallurgical and Materials Transactions B 2014;45:2247-61.

[3] Acharya R, Bansal R, Gambone JJ, Das S. A Microstructure Evolution Model for the Processing of Single-Crystal Alloy CMSX-4 Through Scanning Laser Epitaxy for Turbine Engine Hot-Section Component Repair (Part II). Metallurgical and Materials Transactions B 2014;45:2279-90.

[4] Basak A, Acharya R, Das S. Additive Manufacturing of Single-Crystal Superalloy CMSX-4 Through Scanning Laser Epitaxy: Computational Modeling, Experimental Process Development, and Process Parameter Optimization. Metallurgical and Materials Transactions A 2016;47:3845-59.

[5] Basak A, Das S. A Study on the Effects of Substrate Crystallographic Orientation on Microstructural Characteristics of René N5 Processed through Scanning Laser Epitaxy. Proceedings of the 13th Intenational Symposium of Superalloys 2016:1041-9.

[6] Basak A, Das S. Additive Manufacturing of Nickel-Base Superalloy René N5 through Scanning Laser Epitaxy (SLE) − Material Processing, Microstructures, and Microhardness Properties. Advanced Engineering Materials 2017;19:1600690.

[7] Basak A, Das S. A Study on the Microstructural Characterization of René 142 Deposited Atop René 125 Processed through Scanning Laser Epitaxy. Materials Science Forum 2016;879:187-92.

[8] Basak A, Das S. Microstructure of nickel-base superalloy MAR-M247 additively manufactured through scanning laser epitaxy (SLE). Journal of Alloys and Compounds 2017;705:806-16.

[9] Acharya R, Bansal R, Gambone JJ, Kaplan MA, Fuchs GE, Das S, et al. Additive Manufacturing and Characterization of René 80 Superalloy Processed Through Scanning Laser Epitaxy for Turbine Engine Hot-Section Component Repair. Advanced Engineering Materials 2015;17:942-50.

[10] Acharya R, Das S. Additive Manufacturing of IN100 Superalloy Through Scanning Laser Epitaxy for Turbine Engine Hot-Section Component Repair: Process Development, Modeling, Microstructural Characterization, and Process Control. Metallurgical and Materials Transactions A 2015;46:3864-75.

[11] Basak A, Das S. Additive Manufacturing of Nickel-Base Superalloy IN100 through Scanning Laser Epitaxy (SLE). TMS JOM (Submitted).

[12] Harris K, Erickson G, Sikkenga S, Brentnall W, Aurrecoechea J, Kubarych K. Development of the rhenium containing superalloys CMSX-4® & CM 186 LC® for single crystal blade and directionally solidified Vane applications in advanced turbine engines. Superalloys 1992 1992;297.

[13] Frasier D, Whetstone J, Harris K, Erickson G, Schwer R. Process and alloy optimization for CMSX-4 superalloy single crystal airfoils. High Temperature Materials for Power Engineering 1990:1281-300.

[14] Giamei A, Pearson D, Anton D. γ/γ′: The Key to Superalloy Behavior. MRS Proceedings: Cambridge Univ Press; 1984. p. 293-308.